Discovery of 5-[[4-[(2,3-Dimethyl-2*H*-indazol-6-yl)methylamino]-2-pyrimidinyl]amino]-2-methyl-benzenesulfonamide (Pazopanib), a Novel and Potent Vascular Endothelial Growth Factor Receptor Inhibitor[†]

Philip A. Harris,*,[§] Amogh Boloor,[∥] Mui Cheung,[⊥] Rakesh Kumar,[§] Renae M. Crosby,[‡] Ronda G. Davis-Ward,[‡] Andrea H. Epperly,[‡] Kevin W. Hinkle,[‡] Robert N. Hunter III,[‡] Jennifer H. Johnson,[‡] Victoria B. Knick,[‡] Christopher P. Laudeman,[‡] Deirdre K. Luttrell,[#] Robert A. Mook,[‡] Robert T. Nolte,[‡] Sharon K. Rudolph,[‡] Jerzy R. Szewczyk,[‡] Anne T. Truesdale,[‡] James M. Veal,[▽] Liping Wang,[‡] and Jeffrey A. Stafford[○]

GlaxoSmithKline, Five Moore Drive, Research Triangle Park, North Carolina 27709

Inhibition of the vascular endothelial growth factor (VEGF) signaling pathway has emerged as one of the most promising new approaches for cancer therapy. We describe herein the key steps starting from an initial screening hit leading to the discovery of pazopanib, N^4-(2,3-dimethyl-2*H*-indazol-6-yl)-N^4-methyl-N^2-(4-methyl-3-sulfonamidophenyl)-2,4-pyrimidinediamine, a potent pan-VEGF receptor (VEGFR) inhibitor under clinical development for renal-cell cancer and other solid tumors.

Solid tumors are dependent for growth on nutrients and oxygen they receive via angiogenesis, the process wherein new capillaries are formed from existing blood vessels. This is facilitated by a number of endogenous proteins among which VEGF[a] is thought to be key.[1] VEGF is secreted by tumors and induces a mitogenic response through its binding to one of three tyrosine kinase receptors (VEGFR-1 to -3) on nearby endothelial cells.[2] Thus inhibition of this signaling pathway should block angiogenesis and subsequent tumor growth.[3] The first clinical validation of this hypothesis came from bevacizumab, a monoclonal antibody to VEGF, which is approved for treatment of both metastatic colorectal cancer in combination with 5-fluorouracil, and for nonsmall cell lung cancer in combination with carboplatin and paclitaxel.[4] More recently sorafenib and sunitinib, small-molecule multikinase inhibitors which inhibit the VEGF and platelet-derived growth factor (PDGF) receptor tyrosine kinases among others, have been approved for treatment of advanced renal-cell carcinoma.[5,6] This paper describes the key steps leading to the discovery of pazopanib, N^4-(2,3-

dimethyl-2*H*-indazol-6-yl)-N^4-methyl-N^2-(4-methyl-3-sulfonamidophenyl)-2,4-pyrimidinediamine, a potent pan-VEGFR inhibitor under clinical development as an oral treatment for a variety of solid tumors.[7]

Screening of our sample collection identified N,N''-bis(3-bromoanilino)-5-fluoro-2,4-pyrimidine (**1**) as an inhibitor of VEGFR-2 with an IC$_{50}$ of ~400 nM. In the initial optimization of this series, we employed structure-based design utilizing binding information from another screening hit, 4-(4-methyl-3-hydroxyanilino)-6,7-dimethoxyquinazoline (**2**), which has an IC$_{50}$ value of 0.6 nM against VEGFR-2.[8]

Although considerably more potent than the 2,4-dianilino-pyrimidine **1**, quinazoline **2** was not viewed as attractive a starting point for lead optimization because this template had already been described in the kinase area. Since crystallography data on VEGFR-2 was not available at the time, we utilized a homology model of the kinase domain based on fibroblast growth factor receptor (FGFR) crystal structures to predict the binding modes of both templates.[9] Examination of their respective binding modes indicated the pyrimidine and the quinazoline bind similarly in the ATP binding site. The pyrimidine N-1 and the C-2 anilino N—H were predicted to make hydrogen acceptor and donor bonds with the peptide backbone of Cys919, respectively; while the quinazoline N-1 was predicted to make a hydrogen bond accepting interaction with Cys919, along with the quinazoline C-2 hydrogen making an aromatic CH···O=C interaction to Glu917.[10] In these conformations, both anilines at the C-4 pyrimidine and C-4 quinazoline overlay together and led us to prepare *N*-(3-bromoanilino)-*N'*-(4-methyl-3-hydroxyanilino)-2,4-pyrimidine (**3**) (Figure 1).

Pyrimidine **3** inhibited VEGFR-2 with an IC$_{50}$ of 6.3 nM, representing almost a hundred-fold improvement in binding compared to **1**. This potency increase was attributed to a key predicted hydrogen bond interaction between the phenol hydroxyl and the NH of Asp1046 in the protein backbone (see Figure 2). As a measure of cellular activity, **3** inhibited VEGF-induced proliferation of human umbilical vein endothelial cells (v-HUVEC) with an IC$_{50}$ of 0.54 μM. As a reference, vandetanib, *N*-(4-bromo-2-fluorophenyl)-6-methoxy-7-[(1-methyl-4-piperidinyl)methoxy]-4-quinazolinamine, a VEGFR2 inhibitor currently in late stage clinical evaluation, inhibited v-HUVEC

Figure 1. Structures of pyrimidines **1** and **3** and quinazoline **2**.

Figure 2. Predicted binding mode of quinazoline **2** in yellow overlaid with pyrimidine **3**.
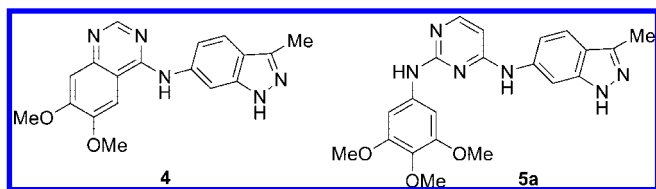
Figure 3. Structure of quinazoline **4** and pyrimidine **5a**.

Figure 4. Medicinal chemistry strategy.

Figure 5. Structure of pyrimidines **5b** and **5c**.

with an IC_{50} of 0.40 μM. Stimulation of HUVEC proliferation with basic fibroblast growth factor (b-FGF) was utilized as a measure of selectivity because this should be unaffected by a VEGFR-2 inhibitor, and in this assay pyrimidine **3** afforded an IC_{50} of 3.5 μM.

Although introduction of the 4-methyl-3-hydroxy aniline at the pyrimidine C-4 position imparted excellent in vitro potency, the pharmacokinetic profile of the 4-(4-methyl-3-hydroxyanilino)-pyrimidines was poor. Moderate to high clearances (28−83 mL/min/kg), presumably due to rapid phase II glucuronidation or sulfation reactions of the phenol functionality and low bioavailabilities (<11%) were observed in the mouse, which would not support the target product profile of a once-daily orally delivered drug. At this stage, cross-screening of in-house kinase inhibitor libraries identified the quinazoline **4** with excellent potency against VEGFR-2 with an IC_{50} of 1.7 nM. The 3-methylindazole appeared to be an equipotent replacement of the 4-methyl-3-hydroxyaniline with reduced potential for glucuronidation. Incorporation of the 3-methylindazole heterocycle into the pyrimidine series yielded indazolylpyrimidine **5a** with good potency against VEGFR-2 ($IC_{50} = 6.3$ nM) and v-HUVECs ($IC_{50} = 0.18$ μM). The pharmacokinetics of **5a** was significantly improved with a clearance of 16 mL/min/kg and an oral bioavailability of 85% at a dose of 10 mg/kg in the rat.

The focus of the medicinal chemistry strategy was to optimize biochemical potency and cell-based selectivity, while simultaneously improving the pharmacokinetic profile to support a once-daily oral therapy. As illustrated in Figures 3–5, the molecule was sectioned into three regions, replacement of the aniline, the core, and the heterocycle. In addition, substitution at the amino nitrogen at C-4 was considered.

Compounds were prepared according to the synthetic sequence outlined in Scheme 1. Thus, *o*-ethylaniline (**6**) was
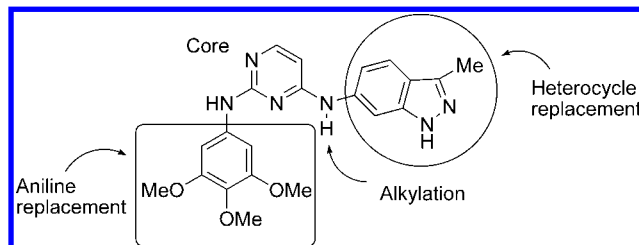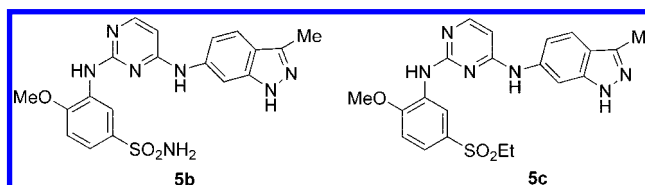
nitrated to yield 2-ethyl-5-nitroaniline (**7**), and this underwent cyclization with isoamyl nitrite in acetic acid to give 3-methyl-6-nitroindazole (**8**). Reduction with tin(II) chloride gave 6-amino-3-methylindazole (**9**) and condensation with 2,4-dichloropyrimidine using basic conditions in THF and ethanol yielded *N*-(2-chloro-4-pyrimidinyl)-3-methylindazol-6-amine (**10**). Finally, a second condensation with various anilines was accomplished using acidic conditions in iso-propanol to yield the desired pyrimidines (**5**).

Keeping the 3-methylindazole constant, a survey of a variety of anilines at the C-2 position of the pyrimidine revealed the 3,4,5-trimethoxy aniline containing pyrimidine **5a** as one of the most potent inhibitors, with the majority of other anilines having diminished activity. Incorporation of a sulfone or sulfonamide at the meta position of the aniline led to comparable potencies. A modest increase in potency in both enzymatic and cellular assays was observed by a combination of a 2-methoxy group with either a 5-sulfonamide (**5b**) or 5-sulfone (**5c**). A similar observation was noted in an earlier series of VEGFR-2 inhibitors we investigated, the 2-anilino-5-phenyl-oxazoles.[11] Molecular modeling, later supported by crystallographic data, proposed that the methoxy group of **5c** sits in a lipophilic pocket and acts to orient the sulfone group to interact with Asn923 as shown in Figure 6. Regarding the role of the 3-methylindazole, the model showed a more direct interaction between the indazole π cloud and the ε amino group of Lys868, as opposed to a hydrogen bond to the NH of Asp1046 as was modeled for the phenol of pyrimidine **3** in Figure 2. This conformation for **5c** was due to the preferred indazole 1H tautomer state disfavoring the Asp 1046 hydrogen bond and was consistent with data observed in subsequent crystal studies. No bridging waters were observed to Asp1046, although sufficient space appeared available. Given the relatively similar measured binding affinities of the 3-methylindazole versus the phenol, the current hypothesis is that that the Lys868−indazole interaction is energetically comparable to that of the Asp 1046−phenol OH interaction.

Scheme 1[a]
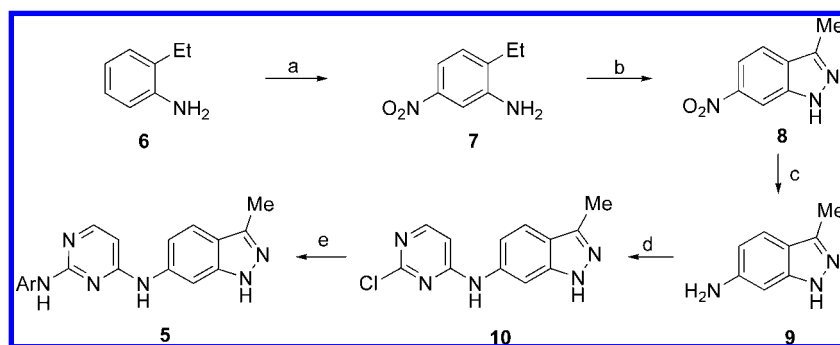
[a] Reagents and conditions: (a) fuming HNO$_3$, conc H$_2$SO$_4$, 60%; (b) isoamyl nitrite, AcOH, 98%; (c) SnCl$_2$, conc HCl, glyme, 92%; (d) 2,4-dichloropyrimidine, NaHCO$_3$, EtOH, THF, rt, 89%; (e) ArNH$_2$, *i*PrOH, HCl, 80 °C, 66−92%.
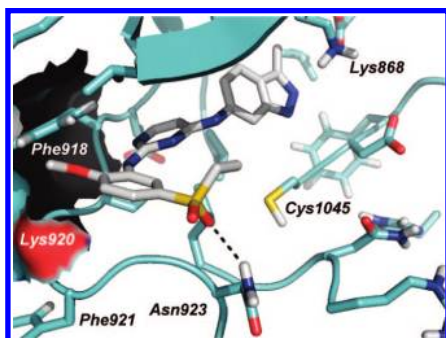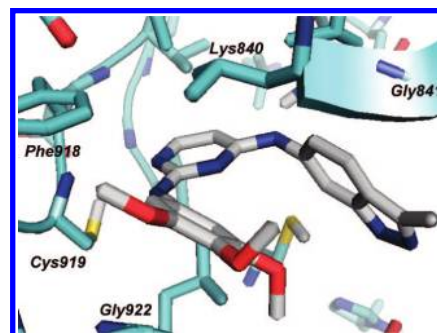

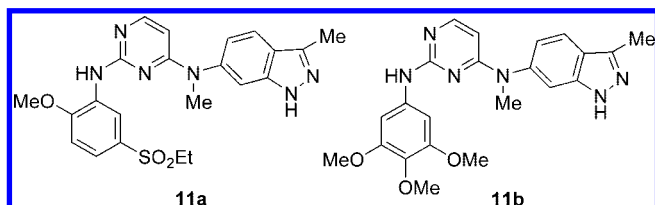**Figure 6.** Predicted binding mode of pyrimidine **5c**.

Figure 7. Structure of pyrimidines **11a** and **11b**.

Pyrimidine **5c** possessed the desired cellular potency and selectivity in VEGF and bFGF driven HUVEC, with IC$_{50}$'s of 0.13 and 13 μM, respectively. In the rat, plasma clearance (40 mL/min/kg) and bioavailability (28%) were moderate.

To examine the potential for substitution at the C-4 amino nitrogen of the pyrimidine, a number of alkylated derivatives were examined. We observed that small alkyl groups were well tolerated, but groups larger than ethyl resulted in loss of potency. While providing comparable enzymatic potency to its unalkylated analogue **5c**, N-methylated inhibitor **11a** (Figure 7) showed an improved pharmacokinetic profile in the rat with lower clearance (10 mL/min/kg) and higher oral bioavailability (65%). This improved profile is likely a result of removal of one of the H-bond donors from the inhibitor because the presence of multiple H-bond donors are known to be detrimental for absorption and potential sites of metabolism.[12]

A crystal structure of pyrimidine **5a** with VEGFR2 confirmed its predicted mode of binding within the ATP site, with the pyrimidine N-1 and the C-2 anilino N−H making hydrogen acceptor and donor bonds with the peptide backbone of Cys919 (Figure 8). Unexpectedly, the electron density map showed the indazole heterocycle residing in two alternative pockets, resulting in both an "S-shaped" conformation with the indazole projected into the back lipophilic pocket as in the model, and a "U-shaped" conformation with the indazole projected out into the ATP binding pocket. On the other hand, a crystal structure

Figure 8. Crystal structure of pyrimidine **5a** with VEGFR-2, with only the "U-shaped" conformation shown.
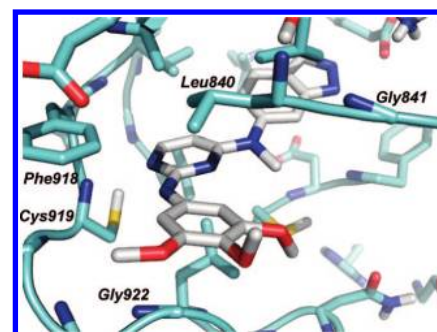
Figure 9. Crystal structure of pyrimidine **11b**.

of the N-methylated pyrimidine analogue **11b** revealed the inhibitor only in an "S-shaped" conformation (Figure 9). Additional crystal structures of indazolylpyrimidines reinforced the trend that unalkylated derivatives displayed U-shaped binding conformations, while N-alkylated derivatives displayed S-shaped conformations. The Schrodinger modeling package was used to explore the conformational space of **5a** and **11b** with the Merck molecular force field (MMFF) model and a dielectric constant of 2. The U-shaped conformation was favored by 0.22 kcal/mol for **5a**, whereas for **11b**, the S-shaped conformation was preferred by 1.10 kcal/mol, most likely to avoid an unfavorable steric interaction between the methyl group and the pyrimidine C-5 hydrogen. These results were also fully consistent with Guassian ab initio calculations on test molecule systems using the 6-31G* basis set.

At this stage, pyrimidines containing the 3-methylindazole heterocycle and methylated at the C-4 amino nitrogen possessed both good in vitro and cross-species pharmacokinetic profiles. However, significant inhibition (IC$_{50}$ <10 μM) was observed against a number of cytochrome P450 isozymes. A possible rationale for this involves binding of the nitrogens on the

Table 1. Effect of Heterocyclic Replacements on P450 Isozymes Inhibition
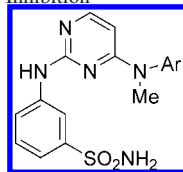
Cpd	Ar	VEGFR2[a] IC$_{50}$ nM	HUVEC[b] IC$_{50}$ μM	Inhibition of P450 Isozymes IC$_{50}$ μM[c]			
				2C9	2C19	2D6	3A4[d]
12a		0.6	0.094	0.7	7.2	4.8	7.6 / 16
12b		36	1.4	1	9.3	6.3	13 / 1.7
12c		5.6	0.023	1.4	20	16	16 / 31
12d		2.6	11	0.5	1.4	66	74 / 79
12e		7.6	0.11	2.9	9.2	18	4.7 / 3.9
12f		63	2.8	15	26	25	26 / 1.7
12g		17	1.4	9	33	33	27 / 45

[a] Inhibition of VEGFR-2-induced proliveration of HUVEC cells; values are means of two or more experiments. [b] VEGF-induced proliferation of HUVEC cells; values are means of two or more experiments. [c] Substrates: CYP2C9, 7-methoxy-4-trifluoromethylcoumarin-3-acetic acid; CYP2C19, 3-butyryl-7-methoxycoumarin; CYP2D6, 4-Methylaminomethyl-7-methoxycoumarin. [d] CYP3A4 substrates: diethoxyfluorescein/7-Benzyloxyquinoline.

indazole heterocycle to the heme iron of the cytochrome P450 enzyme, so one route to diminish such binding would be to add steric hindrance to the heterocycle ring.[13] This led us to examine a number of more sterically hindered heterocycles as replacements for the 3-methylindazole, as exemplified in Table 1 for a set of inhibitors **12a**−**g** with the aniline held constant as 3-aminobenzene sulfonamide.

Although the P450 profile was improved in a number of cases, the majority of heterocyclic replacements led to diminution of cellular activity. Addition of a methyl group at the 2-position of the indazole (pyrimidine **12c**) gave improved cellular efficacy against v-HUVEC cells and a better profile against the CYP2C19, CYP2D6, and CYP3A4 isozymes as compared to pyrimidine **12a**, although CYP2C9 remained unchanged. Because of these factors, the 2,3-dimethylindazole was chosen as the preferred heterocycle.

With the 2,3-dimethylindazole preferred, a second aniline survey at the C-2 position of the pyrimidine was undertaken with a focus on sulfonamide and sulfone substituted anilines. This identified the indazolylpyrimidine (**13**, Figure 10) possessing a meta primary sulfonamide and a para methyl group at the aniline as possessing a desirable combination of cellular potency and selectivity in VEGF and bFGF driven HUVEC, with IC$_{50}$'s of 0.021 and 0.72 μM, respectively.

Pyrimidine **13** showed good potency against all the human VEGFR receptors with an IC$_{50}$ of 10, 30, and 47 nM for VEGFR-1, -2, and -3, respectively. Significant activity was also seen against the closely related tyrosine receptor kinases
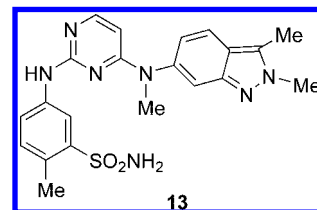
Figure 10. Structure of indazolylpyrimidine **13**.

PDGFRβ, c-Kit, FGF-R1, and c-fms with IC$_{50}$'s of 84, 74, 140, and 146 nM, respectively. In cellular assays, in addition to inhibiting the VEGF-induced proliferation of HUVECs, pyrimidine **13** potently inhibited VEGF-induced phosphorylation of VEGFR-2 in HUVEC cells with an IC$_{50}$ of ∼8 nM. Pyrimidine **13** possessed good pharmacokinetics in rat, dog, and monkey with low clearances (1.4−1.7 mL/min/kg) and good oral bioavailabilities (72, 47, 65%) dosed at 10, 1, and 5 mg/kg, respectively.[14] The cytochrome P450 profile was also improved with inhibition >10 μM against the isozymes tested, with the exception of 2C9 (7.9 μM).

As a measure of its ability to inhibit angiogenesis in vivo, pyrimidine **13** was examined in the mouse matrigel plug assay. In this assay, a gel plug of extracellular matrix containing b-FGF, which gives a more robust angiogenic response than VEGF in this assay format, is implanted subcutaneously to stimulate vascularization inside the plug. The plug is then removed after 5 days, and the vascularization of this plug is estimated by determination of the hemoglobin content. Follow-

Table 2. Mouse Oral Exposures and Xenograft Tumor Growth Inhibition by Pyrimidine **13**

				tumor model (% inhibition)[a]		
dose (mg/kg)	AUC_{0-inf} ($\mu g \cdot h/mL$)	plasma conc @ 12 h (ng mL)	inhibition of angiogenesis (Matrigel plug assay, %)	HT29	A375P	HN5
10	220	6320	0	32	16	99
30	657	24831	57	59	35	102
100	1141	38538	83	69	55	110

[a] Inhibition of tumor growth compared to vehicle treated mice from independent experiments.

ing once-daily oral administration of pyrimidine **13**, angiogenesis was inhibited in a dose-dependent manner (Table 2). The oral exposure increased in a dose-proportional manner on going from a 10 to 30 mg/kg dose with a reduced increase in exposure observed in going from the 30 to 100 mg/kg dose level. Pyrimidine **13** was also examined in a second animal model of angiogenesis, the mouse corneal micropocket assay, in which ocular angiogenesis is induced by implantation of slow release pellets of VEGF into the mouse cornea. Treatment of mice with 100 mg/kg of **13** twice daily for five days resulted in significant inhibition in the degree of vascularization.[14] The antiangiogenic activity of pyrimidine **13** was examined in mice bearing established human xenografts (200−250 mm³) using HT29 (colon carcinoma), A375P (melanoma), and HN5 (head and neck carcinoma) tumors following a standard three-week course of therapy. The HN5 and HT29 xenografts responded better at all doses compared to the A375P model, which is historically more resistant to VEGFR-2 inhibitors (Table 2).[15] As support that the observed inhibition of xenograft growth is working through an antiangiogenic rather than antitumor mechanism, no antiproliferative activity was observed below 10 μM for **13** against these human tumor lines (HT29, HN5, A375P) growing in serum-containing media. No significant effect on the body weight of mice was observed, and the animals appeared healthy and active throughout the study duration.

A study in mice examining the pharmacokinetics of pyrimidine **13** administered as an oral bolus demonstrated that the antitumor and antiangiogenic activity of the agent requires a threshold steady-state plasma concentration ≥40 μM that is similar to the concentration required for inhibition of VEGF-induced VEGFR-2 phosphorylation in mouse lung in vivo.[14] The discrepancy between the in vivo required concentration and in vitro potency against v-HUVEC can be attributed to the high protein binding for **13** of >99.9% as measured by equilibrium dialysis.

On the basis of its favorable pharmokinetic profiles and in vivo efficacies, the mono-HCl salt of pyrimidine **13** (pazopanib) was progressed into full development. It is currently being evaluated as an oral treatment for renal-cell cancer and other solid tumors with ongoing phase II and phase III clinical studies.[16]

Experimental Section

All purchased starting materials were used without further purification. ¹H NMR spectra were recorded on either a Varian VXR-300, a Varian Unity-300, or a Varian Unity-400 instrument as solutions in DMSO-d_6 (unless otherwise stated). Chemical shifts are expressed in parts per million (ppm, δ units). Coupling constants are in units of hertz (Hz). Splitting patterns describe apparent multiplicities and are designated as s (singlet), d (doublet), t (triplet), q (quartet), m (multiplet), br s (broad singlet). LCMS APCI were recorded on an Agilent LC/MSD SL, UV detector monitoring at 254 nm using a Zorbax XDB-C8 column (4.6 mm × 75 mm, 3.5 μm), 5−95% CH₃CN:H₂O (with 0.1% TFA) over 4 min and hold for 1 min; flow rate = 2 mL/min at 40 °C. Method A was performed on a Agilent 1100 series, UV detector monitoring at 254 nm using a Zorbax SB-C8 column (4.6 mm × 150 mm, 5 μm), 5−100%

CH₃CN:H₂O (with 0.02% TFA) over 12.5 min and hold for 2.5 min, flow rate = 1.5 mL/min at 40 °C. Method B was performed on a Agilent 1100 series, UV detector monitoring at 254 nm using a Zorbax XDB-C8 column (4.6 mm × 75 mm, 3.5 μm), 5−95% CH₃CN:H₂O (with 0.1% TFA) over 4 min and hold for 1 min, flow rate = 2 mL/min at 40 °C. Method C was performed on a Agilent 1200 series, UV detector monitoring at 260 nm using a Phenomenex C18 column (4.6 mm × 150 mm, 3 μm), 5−95% CH₃CN:H₂O (with 0.1% TFA) over 20 min and hold for 5 min, flow rate = 1 mL/min at 40 °C. Elemental analyses were carried out by Quantitative Technologies Inc., Whitehouse, NJ. Compounds **1** and **2** were prepared as described previously from condensation of 5-fluoro-2,4-dichloropyrimidine and 3-bromoaniline, and 4-chloro-6,7-dimethoxyquinazoline and 3-hydroxy-4-methylaniline, respectively.[17,18]

2-(3-Bromoanilino)-4-(3-hydroxy-4-methylanilino)pyrimidine Hydrochloride (3). To a stirred solution of 5-amino-o-cresol (0.42 g, 3.4 mmol) and NaHCO₃ (0.85 g, 10 mmol) in EtOH (15 mL) was added 2,4-dichloropyrimidine (0.50 g, 3.4 mmol) at room temperature. The reaction was refluxed for 1 h, and on cooling, the resulting suspension was filtered and the residue washed thoroughly with EtOH. The filtrate was diluted with hexanes to precipitate a second batch of product. The combined batches were washed with EtOH and dried to afford 2-chloro-4-(3-hydroxy-4-methylanilino)pyrimidine (0.58 g, 73% yield). ¹H NMR (400 MHz): δ 9.82 (s, 1H), 9.43 (s, 1H), 8.10 (d, 1H, $J = 7.0$ Hz), 7.03 (m, 1H), 6.88 (m, 1H), 6.68 (d, 1H, $J = 7.0$ Hz), 3.34 (s, 3H). LCMS (ES, m/z) 236, 238 (M + H⁺).

A stirred mixture of 2-chloro-4-(3-hydroxy-4-methylanilino)pyrimidine (0.10 g, 0.42 mmol) and 3-bromoaniline (0.081 g, 0.47 mmol) in EtOH (15 mL) was reflux for 16 h. Upon cooling the reaction, the precipitated solid was filtered off, washed with EtOAc and hexanes, and dried under vacuum to give **3** (0.05 g, 29% yield). ¹H NMR (400 MHz): δ 10.32−10.62 (br m, 2H), 9.49 (br s, 1H), 7.96 (d, 1H, $J = 7.0$ Hz), 7.87 (s, 1H), 7.50 (d, 1H, $J = 6.8$ Hz), 7.26−7.35 (m, 2H), 7.10 (d, 1H, $J = 1.6$ Hz), 7.02−7.08 (m, 1H), 6.81 (d, 1H, $J = 0.6$ Hz), 6.40 (d, 1H, $J = 6.9$ Hz), 2.09 (s, 3H). LCMS (APCI, m/z) 371, 373 (M⁺).

N-(3-Methyl-1H-indazol-6-yl)-6,7-bis(methyloxy)-4-quinazolinamine Hydrochloride (4). Prepared from 4-chloro-6,7-dimethoxyquinazoline and **9** in 90% yield by the procedure described in the preparation of **3** using iPrOH as solvent and a reaction time of 90 min. ¹H NMR (400 MHz): δ 12.8 (br s, 1 H), 11.3 (br s, 1 H), 8.84 (s, 1 H), 8.28 (s, 1 H), 7.85 (d, $J = 1.0$ Hz, 1 H), 7.79 (d, $J = 8.6$ Hz, 1 H), 7.37 (dd, $J = 8.6, 1.5$ Hz, 1 H), 7.34 (s, 1 H), 4.03 (s, 3 H), 4.01 (s, 3 H), 2.52 (s, 3 H). LCMS (APCI, m/z) 336 (M + H⁺). Anal. (C₁₈H₁₇N₅O₂·HCl·0.4H₂O) C, H, N.

N-(2-Chloro-4-pyrimidinyl)-N-(3-methyl-1H-indazol-6-yl)amine (10). To a solution of 2-ethyl-5-nitroaniline[19] (**7**) (10.0 g, 60 mmol) in glacial AcOH (300 mL) at room temperature, was added dropwise a solution of $tert$-butyl nitrite (9.0 mL, 60 mmol) in AcOH (40 mL) over 15 min. After the addition was complete, the solution was allowed to stir for 30 min. The AcOH was removed in vacuo to afford an orange solid. The solid was taken up in EtOAc (120 mL) and washed with saturated aqueous NaHCO₃ (3 × 100 mL). The organic layer was dried over MgSO₄, filtered, and the solvent was removed in vacuo to afford 3-methyl-6-nitroindazole (**8**) as a yellow solid (10.4 g, 98% yield).

To a stirred solution of **8** (10.4 g, 59 mmol) in 2-methoxyethyl ether (100 mL) at 0 °C was added dropwise a solution of tin(II) chloride (45.0 g, 240 mmol) in concentrated HCl (86 mL) over 15

min, maintaining the reaction temperature below 100 °C with an ice bath. After the addition was complete, the ice bath was removed and the solution was allowed to stir for an additional 20 min. Addition of Et$_2$O (70 mL) to the solution resulted in formation of a yellow precipitate, which was filtered off, washed with Et$_2$O, and dried to afford 6-amino-3-methylindazole (**9**) (10.0 g, 92% yield). ^{1}H NMR (400 MHz): δ 9.5 (br s, 1H), 7.79 (d, 1H, J = 8.6 Hz), 7.44 (s, 1H), 7.02 (d, 1H, J = 8.6 Hz), 3.5 (br s, 2H), 2.50 (s, 3H). LCMS (APCI, m/z) 148 (M + H$^+$).

To a stirred solution of **9** (2.7 g, 15 mmol) and NaHCO$_3$ (1.3 g, 45 mmol) in THF (15 mL) and EtOH (60 mL) was added 2,4-dichloropyrimidine (6.7 g, 45 mmol) at room temperature. The reaction was stirred for 4 h, and the resulting suspension was filtered and the residue washed thoroughly with EtOH. The filtrate was concentrated under reduced pressure, and the resulting solid was washed with Et$_2$O to remove excess 2,4-dichloropyrimidine to afford **10** (3.5 g, 89% yield). ^{1}H NMR (400 MHz): δ 12.56 (s, 1 H), 10.14 (s, 1 H), 8.18 (d, J = 6.1 Hz, 1 H), 8.00 (br s, 1 H), 7.65 (d, J = 8.6 Hz, 1 H), 7.08 (dd, J = 8.7, 1.6 Hz, 1 H), 6.81 (d, J = 6.1 Hz, 1 H), 2.46 (s, 3 H). LCMS (APCI, m/z) 260, 262 (M + H$^+$). HPLC (method A): 96% (t_R 6.3 min).

N^4-(3-Methyl-1H-indazol-6-yl)-N^2-[3,4,5-tris(methyloxy)phenyl]-2,4-pyrimidinediamine (5a). Prepared from **10** and 3,4,5-trimethoxyaniline by the procedure described in the preparation of **3**, and the filtered product was further purified by silica gel chromatography eluting with a hexanes/EtOAc to yield **5a** in 83% yield. ^{1}H NMR (400 MHz): δ 12.55 (br s, 1H), 10.89 (br s, 1H), 10.41 (br s, 1H), 7.93 (d, 1H, J = 6.7 Hz), 7.69 (br s, 1H), 7.63 (br s, 1H), 7.33−7.41 (m, 1H), 6.82 (br s, 2H), 6.48 (d, 1H, J = 6.7 Hz), 3.65 (s, 3H), 3.58 (s, 6H), 2.47 (s, 3H). LCMS (APCI, m/z) 407 (M + H$^+$).

4-Methoxy-3-({4-[(3-methyl-1H-indazol-6-yl)amino]-2-pyrimidinyl}amino)benzenesulfonamide (5b). Prepared from **10** and 3-amino-4-methoxybenzenesulfonamide by the procedure described in the preparation of **3**, and the filtered product was further purified by silica gel chromatography eluting with a hexanes/EtOAc to yield **5b** in 89% yield. ^{1}H NMR (400 MHz): δ 12.28 (br s, 1H), 9.56 (br s, 1H), 8.72 (br s, 1H), 8.02 (d, 1H, J = 5.7 Hz), 7.87 (br s, 1H), 7.74 (br s, 1H), 7.55 (d, 1H, J = 8.7 Hz), 7.43 (d, 1H, J = 8.0 Hz), 7.17 − 7.13 (m, 4H), 6.32 (d, 1H, J = 5.9 Hz), 3.91 (s, 3H), 2.39 (s, 3H). LCMS (APCI, m/z) 424 (M − H$^+$).

N^2-[2-Methoxy-5-(ethylsulfonyl)phenyl]-N^4-(3-methyl-1H-indazol-6-yl)-2,4-pyrimidinediamine Hydrochloride (5c). Prepared from **10** and 5-ethylsulfonyl-2-methoxyaniline in 90% yield by the procedure described in the preparation of **3**. ^{1}H NMR (400 MHz): δ 12.42 (s, 1H), 10.60 (s, 1H), 8.85 (d, J = 2.2 Hz, 1H), 8.81 (d, J = 5.8 Hz, 1H), 7.92 (bs, 1H), 7.82 (s, 1H), 7.60 (d, J = 8.6 Hz, 1H), 7.55 (dd, J = 8.5, 2.3 Hz, 1H), 7.28 (d, J = 8.7 Hz, 1H), 7.21 (d, J = 8.6 Hz, 1H), 6.39 (d, J = 5.8 Hz, 1H), 3.96 (s, 3H), 3.07 (q, J = 7.4 Hz, 2H), 2.50 (s, 3H), 1.03 (t, J = 7.4 Hz, 3H). LCMS (EI, m/z) 439 (M + H$^+$).

N^2-[5-(Ethylsulfonyl)-2-methoxyphenyl]-N^4-methyl-N^4-(3-methyl-1H-indazol-6-yl)-2,4-pyrimidinediamine (11a). To a solution of **10** (2.8 g, 11 mmol), triethylamine (1.5 mL, 11 mmol) and 4-dimethylaminopyridine (0.13 g, 1.1 mmol) in a mixture of MeCN (14 mL) and DMF (50 mL) was added di-*tert*-butyl dicarbonate (2.36 g, 11 mmol) portion wise over 3 min. After stirring for 1 h, the solution was diluted with water and extracted with Et$_2$O (3 × 40 mL). The combined extracts were dried over Na$_2$SO$_4$, filtered, and concentrated in vacuo. The resulting residue was purified by silica gel column chromatography eluting with CH$_2$Cl$_2$/EtOAc (9: 1) to give *tert*-butyl 6-[(2-chloro-4-pyrimidinyl)amino]-3-methyl-1H-indazole-1-carboxylate (3.3 g, 85% yield). ^{1}H NMR (400 MHz): δ 10.35 (s, 1 H), 8.39 (d, J = 1.3 Hz, 1 H), 8.23 (d, J = 5.8 Hz, 1 H), 7.80 (d, J = 8.6 Hz, 1 H), 7.55 (dd, J = 8.6, 1.8 Hz, 1 H), 6.85 (d, J = 5.8 Hz, 1 H), 2.50 (s, 3 H), 1.64 (s, 9 H). LCMS (APCI, m/z) 374, 376 (M + H$^+$). HPLC (method A): 99% (t_R 9.5 min).

To a stirred solution of *tert*-butyl 6-[(2-chloro-4-pyrimidinyl)-amino]-3-methyl-1H-indazole-1-carboxylate (3.3 g, 8.8 mmol) in DMF (44 mL) was added NaH (0.23 g, 9.6 mmol) portion wise

over 3 min at room temperature. After 15 min, iodomethane (1.37 g, 9.6 mmol) was added dropwise and stirring continued for 30 min, the reaction was then quenched with water and extracted with ether (3 × 30 mL). The combined extracts were dried over Na$_2$SO$_4$, filtered, and concentrated under reduced pressure to yield a yellow solid. The resulting solid was purified by silica gel column chromatography eluting with CH$_2$Cl$_2$ to yield *tert*-butyl 6-[(2-chloro-4-pyrimidinyl)(methyl)amino]-3-methyl-1H-indazole-1-carboxylate (3.26 g, 95% yield). ^{1}H NMR (400 MHz): δ 8.03 (d, J = 6.1 Hz, 1 H), 7.99 (d, J = 1.5 Hz, 1 H), 7.38 (dd, J = 8.3, 1.8 Hz, 1 H), 7.97 (d, J = 8.3 Hz, 1 H), 6.45 (d, J = 6.1 Hz, 1 H), 3.47 (s, 3 H), 2.55 (s, 3 H), 1.61 (s, 9 H). LCMS (APCI, m/z) 360 (M + H$^+$). HPLC (method A): 90% (t_R 8.4 min).

A solution of *tert*-butyl 6-[(2-chloro-4-pyrimidinyl)(methyl)-amino]-3-methyl-1H-indazole-1-carboxylate (2.0 g, 5.4 mmol) and 5-(ethylsulfonyl)-2-methoxyaniline (1.28 g, 6.0 mmol) in *i*PrOH (11 mL) was stirred for 16 h. The reaction solution was concentrated in vacuo and the residue was dissolved in a 1:1 mixture of CH$_2$Cl$_2$ and trifluoroacetic (40 mL) and stirred for 30 min. The reaction was neutralized by addition of saturated aqueous NaHCO$_3$ and the organic phase separated and the aqueous phase further extracted with CH$_2$Cl$_2$ (100 mL). The combined organic layers were dried over anhydrous MgSO$_4$, filtered, and evaporated to give a crude mixture that was purified by silica gel chromatography eluting with CH$_2$Cl$_2$/MeOH (95:5 v/v) to give **11a** (1.4 g, 57% yield). ^{1}H NMR (400 MHz): δ 12.74 (s, 1H), 9.10 (s, 1H), 7.85 (d, J = 6.0 Hz, 1H), 7.81 (s, 1H), 7.79 (d, J = 8.2 Hz, 1H), 7.46 (d, J = 8.6 Hz, 1H), 7.41 (s, 1H), 7.25 (d, J = 8.2 Hz, 1H), 7.05 (d, J = 8.6 Hz, 1H), 5.78 (d, J = 6.0 Hz, 1H), 3.99 (s, 3H), 3.51 (s, 3H), 3.18 (q, J = 7.4 Hz, 2H), 2.50 (s, 3H), 1.09 (t, J = 7.4 Hz, 3H). LCMS (APCI, m/z) 451, 452 (M + H$^+$). Anal. (C$_{22}$H$_{24}$N$_6$O$_3$S·0.3H$_2$O) C, H, N, S.

N^4-Methyl-N^4-(3-methyl-1H-indazol-6-yl)-N^2-[3,4,5-tris(methyloxy)phenyl]-2,4-pyrimidinediamine (11b). To a solution of *tert*-butyl 6-[(2-chloro-4-pyrimidinyl)(methyl)amino]-3-methyl-1H-indazole-1-carboxylate (0.25 g, 0.67 mmol) and 3,4,5-trimethoxyaniline (0.14 g, 0.74 mmol) in *i*PrOH (6 mL) was added 3 drops of conc HCl and the mixture heated to reflux for 16 h. The mixture was cooled to room temperature, and the resulting precipitate was collected via filtration and washed with *i*PrOH to yield **11b** (0.16 g, 52% yield) as a white solid. ^{1}H NMR (400 MHz): δ 12.67 (br s, 1 H), 9.04 (br s, 1 H), 7.75 (dd, J = 7.5 Hz, 2 H), 7.35 (s, 1 H), 7.15 (s, 2 H), 6.96 (d, J = 8.1 Hz, 1 H), 5.68 (d, J = 7.1 Hz, 1 H), 3.65 (s, 6 H), 3.55 (s, 3 H), 3.46 (s, 3 H), 3.27 (s, 3 H). LCMS (APCI, m/z) 421 (M + H). Anal. (C$_{22}$H$_{24}$N$_6$O$_3$·HCl·0.5H$_2$O) C, H, N, Cl.

3-({4-[Methyl(3-methyl-1H-indazol-6-yl)amino]-2-pyrimidinyl}amino)benzenesulfonamide Hydrochloride (12a). To a solution of *tert*-butyl 6-[(2-chloro-4-pyrimidinyl)(methyl)amino]-3-methyl-1H-indazole-1-carboxylate (0.20 g, 0.54 mmol) and 3-aminobenzenesulfonamide (0.092 g, 0.54 mmol) in *i*PrOH (6 mL) was added 4 drops of conc HCl and the mixture heated to reflux for 16 h. The mixture was cooled to room temperature and diluted with Et$_2$O (6 mL). The resulting precipitate was collected via filtration and washed with Et$_2$O to yield **12a** (0.21 g, 87% yield) as an off-white solid. ^{1}H NMR (300 MHz): δ 12.73 (br s, 1H), 9.54 (s, 1H), 8.55 (s, 1H), 7.86 (d, J = 6.0 Hz, 1H), 7.78−7.81 (m, 2H), 7.40 (s, 1H), 7.33−7.34 (m, 2H), 7.25 (br s, 2H), 7.02 (d, J = 8.4 Hz, 1H), 5.82 (d, J = 6.0 Hz, 1H), 3.51 (s, 3H), 2.50 (s, 3H). LCMS (APCI, m/z) 410 (M + H$^+$).

3-({4-[(1,3-Dimethyl-1H-indazol-6-yl)(methyl)amino]-2-pyrimidinyl}amino)benzenesulfonamide (12b) Hydrochloride. NaH (0.33 g, 14 mmol) was added portion-wise to a solution of **10** (1.2 g, 4.6 mmol) in DMF (12 mL) and the reaction solution stirred at room temperature for 15 min. Iodomethane (0.67 mL, 11 mmol) was then added and the mixture was stirred for a further 30 min. The reaction mixture was then diluted with water (100 mL) and extracted with Et$_2$O (100 mL). The organic layer was dried over Na$_2$SO$_4$, filtered, and evaporated to yield a crude product that was subjected to silica gel chromatography eluting with CH$_2$Cl$_2$/EtOAc (6:4 v/v) to give *N*-(2-chloro-4-pyrimidinyl)-*N*,1,3-trimethyl-1H-

indazol-6-amine (0.80 g, 46% yield), as the major product. ^{1}H NMR (400 MHz, MeOD): δ 7.87 (d, *J* = 6.1 Hz, 1 H), 7.85 (d, *J* = 8.3 Hz, 1 H), 7.53 (d, *J* = 1.0 Hz, 1 H), 7.05 (dd, *J* = 8.5, 1.6 Hz, 1 H), 6.28 (d, *J* = 6.3 Hz, 1 H), 4.00 (s, 3 H) 3.56 (s, 3 H) 2.58 (s, 3 H). LCMS (APCI, *m/z*) 288, 290 (M + H^{+}). HPLC (method A): 99% (*t*R 8.1 min).

Further elution afforded *N*-(2-chloro-4-pyrimidinyl)-*N*,2,3-trimethyl-2*H*-indazol-6-amine (0.20 g, 12% yield) as a minor byproduct. ^{1}H NMR (400 MHz): δ 7.94 (d, *J* = 6.0 Hz, 1H), 7.80 (d, *J* = 7.0 Hz, 1H), 7.50 (d, *J* = 1.0 Hz, 1H), 6.88 (m, 1H), 6.24 (d, *J* = 6.2 Hz, 1H), 4.06 (s, 3H), 3.42 (s, 3H), 2.62 (s, 3H). LCMS (APCI, *m/z*) 288, 290 (M + H^{+}). HPLC (method A): 99% (*t*R 7.3 min).

To a solution of *N*-(2-chloro-4-pyrimidinyl)-*N*,1,3-trimethyl-1*H*-indazol-6-amine (0.20 g, 0.69 mmol) and 3-aminobenzenesulfonamide (0.12 g, 0.69 mmol) in EtOH (15 mL) was added 2 drops of conc HCl, and the mixture was heated to reflux with stirring for 16 h. The mixture was allowed to cool to room temperature and the resulting precipitate was collected via filtration and washed with EtOH to yield **12b** (0.21 g, 66% yield). ^{1}H NMR (400 MHz): δ 10.61 (br s, 1 H), 8.37 (br s, 1 H), 7.88 (d, *J* = 8.6 Hz, 2 H), 7.71 (d, *J* = 1.0 Hz, 2 H), 7.56 (br s, 2 H), 7.41 (s, 2 H), 7.09 (dd, *J* = 8.5, 1.6 Hz, 1 H), 5.97 (br s, 1 H), 3.97 (s, 3 H), 3.59 (s, 3 H). LCMS (APCI, *m/z*) 424 (M + H^{+}). Anal. (C20H21N7O2S·HCl·H2O) C, H, N, Cl, S.

3-({4-[(2,3-Dimethyl-2*H*-indazol-6-yl)(methyl)amino]pyrimidin-2-yl}amino)benzenesulfonamide Dihydrochloride (12c). To a stirred solution of **8** (18.5 g, 110 mmol) in acetone (350 mL) under argon was added trimethyloxonium tetraflouroborate (20 g, 140 mmol). After the solution was allowed to stir for 3 h, the solvent was removed under reduced pressure. To the resulting solid was added saturated aqueous NaHCO3 (600 mL) and a 4:1 mixture of CHCl3/*i*PrOH (200 mL), and the mixture was agitated and the layers were separated. The aqueous phase was extracted with additional CHCl3/*i*PrOH (4 × 200 mL) and the combined organic phases were dried over Na2SO4. Filtration and removal of solvent gave a tan solid that was washed with EtOH (200 mL) to afford 2,3-dimethyl-6-nitro-2*H*-indazole as a yellow solid (13.5 g, 67% yield). ^{1}H NMR (300 MHz): δ 8.51 (s, 1H), 7.94 (d, *J* = 9.1 Hz, 1H), 7.73 (d, *J* = 8.9 Hz, 1H), 4.14 (s, 3H), 2.67 (s, 3H). LCMS (APCI, *m/z*) 192 (M + H^{+}).

2,3-Dimethyl-6-nitro-2*H*-indazole (1.13 g, 5.9 mmol) was dissolved in 2-methoxyethyl ether (12 mL), cooled to 0 °C, and a solution of tin(II) chloride (4.5 g, 0.023 mol) in conc HCl (8.9 mL) was added dropwise over 5 min. On completion, the ice bath was removed and the solution was allowed to stir for an additional 30 min. Et2O (40 mL) was added to the reaction solution resulting in precipitate formation. The precipitate was isolated by filtration and washed with Et2O to afforded 2,3-dimethyl-2*H*-indazol-6-amine hydrochloride (1.1 g, 95% yield) as a yellow solid. ^{1}H NMR (300 MHz): δ 7.77 (d, *J* = 8.9 Hz, 1H), 7.18 (s, 1H), 7.88 (m, 1H), 4.04 (s, 3H), 2.61 (s, 3H). LCMS (APCI, *m/z*) 162 (M + H^{+}).

To a stirred solution of 2,3-dimethyl-2*H*-indazol-6-amine hydrochloride (2.97 g, 15 mmol) and NaHCO3 (5.05 g, 60 mol) in THF (15 mL) and EtOH (60 mL) was added 2,4-dichloropyrimidine (6.70 g, 45 mmol) at room temperature. The reaction was stirred for 4 h at 85 °C and then cooled to room temperature, filtered, and the residue washed thoroughly with EtOAc. The filtrate was concentrated under reduced pressure, and the resulting solid was triturated with EtOAc to yield *N*-(2-chloropyrimidin-4-yl)-2,3-dimethyl-2*H*-indazol-6-amine (3.84 g, 89% yield). ^{1}H NMR (400 MHz): δ 10.25 (br s, 1 H), 8.14 (d, *J* = 5.8 Hz, 1 H), 7.99 (br s, 1 H), 7.62 (d, *J* = 8.8 Hz, 1 H), 6.87 (d, *J* = 6.1 Hz, 1 H), 7.04 (d, *J* = 8.8 Hz, 1 H), 4.01 (s, 3 H), 2.57 (s, 3 H). LCMS (APCI, *m/z*) 274, 276 (M + H^{+}). HPLC (method A): 99% (*t*R 5.8 min).

To a stirred solution of *N*-(2-chloro-4-pyrimidinyl)-2,3-dimethyl-2*H*-indazol-6-amine (7.37 g, 27 mmol) in DMF (50 mL) was added Cs2CO3 (17.60 g, 54 mmol) and methyl iodide (1.84 mL, 30 mmol) at room temperature, and the reaction stirred at room temperature for 16 h. The reaction mixture was poured into an ice−water bath, and the resulting precipitate was filtered off, washed with water,

and air-dried to afford *N*-(2-chloropyrimidin-4-yl)-*N*,2,3-trimethyl-2*H*-indazol-6-amine as an off-white solid (6.43 g, 83%). Analytical data corresponds to that obtained as the minor byproduct from methylation of **10** described in preparation of **12b**.

Condensation of *N*-(2-chloropyrimidin-4-yl)-*N*,2,3-trimethyl-2*H*-indazol-6-amine with 3-benzenesulfonamide following the procedure described in the preparation of **12b** afforded **12c** in 92% yield as a white solid. ^{1}H NMR (400 MHz, DMSO-*d*6 + NaHCO3): δ 9.58 (br s, 1H), 8.55 (br s, 1H), 7.83 (d, *J* = 6.2 Hz, 1H), 7.74−7.79 (m, 2H), 7.43 (s, 1H), 7.34−7.37 (m, 2H), 7.24 (s, 2H), 6.86 (m, 1H), 5.77 (d, *J* = 6.1 Hz, 1H), 4.04 (s, 3H), 3.48 (s, 3H), 2.61 (s, 3H). LCMS (APCI, *m/z*) 424 (M + H^{+}). Anal. (C20H21N7O2S·2HCl·1.5H2O) C, H, N, Cl, S.

3-[(4-{Methyl[3-methyl-2-(benzyl)-2*H*-indazol-6-yl]amino}-2-pyrimidinyl)amino]benzenesulfonamide Hydrochloride (12d). *tert*-Butyl 6-[(2-chloro-4-pyrimidinyl)(methyl)amino]-3-methyl-1*H*-indazole-1-carboxylate (0.5 g, 1.3 mmol) was stirred in a 1:1 mixture of trifluoroacetic acid and CH2Cl2 (4 mL) at room temperature for 16 h. The solvent mixture was evaporated off and residue dissolved into CH2Cl2 (100 mL), washed with saturated aqueous NaHCO3 (100 mL), and the aqueous phase further extracted with CH2Cl2 (100 mL). The organic layers were combined, dried over anhydrous MgSO4, filtered, and evaporated, and the resultant solid was dried in vacuo to give *N*-(2-chloropyrimidin-4-yl)-*N*,3-dimethyl-1*H*-indazol-6-amine as an off-white solid (0.36 g, 100% yield). ^{1}H NMR (300 MHz): δ 12.80 (br s, 1H), 7.94 (d, *J* = 6.0 Hz, 1H), 7.82 (d, *J* = 8.5 Hz, 1H), 7.44 (s, 1H), 7.01 (m, 1H), 6.25 (d, *J* = 6.0 Hz, 1H), 3.42 (s, 3H), 2.50 (s, 3H). LCMS (APCI, *m/z*) 274, 276 (M + H^{+}). HPLC (method A): 99.5% (*t*R 7.2 min).

To a solution of *N*-(2-chloropyrimidin-4-yl)-*N*,3-dimethyl-1*H*-indazol-6-amine (0.36 g, 1.3 mmol) in DMF (4 mL) was added Cs2CO3 (1.11 g, 9 mmol) and benzyl chloride (0.20 g, 1.5 mmol) and the reaction stirred at room temperature for 4 h. The reaction solution was diluted with EtOAc (100 mL) and washed with water (100 mL). The organic layer was separated and the aqueous layer was extracted further with EtOAc (2 × 100 mL). The combined organic layers were dried over anhydrous MgSO4, filtered, and evaporated to give the crude mixture as an oil (0.49 g). Purification by silica gel chromatography eluting with hexanes with increasing EtOAc (0−50%) yielded 1-(benzyl)-*N*-(2-chloropyrimidin-4-yl)-*N*,3-dimethyl-1*H*-indazol-6-amine as the major product (0.36 g, 74% yield) as a white solid. ^{1}H NMR (400 MHz): δ 7.96 (d, *J* = 6.1 Hz, 1 H), 7.83 (d, *J* = 8.6 Hz, 1 H), 7.78 (d, *J* = 1.3 Hz, 1 H), 7.32 (s, 1 H), 7.29 (d, *J* = 6.1 Hz, 1 H), 7.24−7.27 (m, 3 H), 7.07 (dd, *J* = 8.5, 1.6 Hz, 1 H), 6.28 (d, *J* = 6.1 Hz, 1 H), 5.55 (s, 2 H), 3.44 (s, 3 H), 2.51 (s, 3 H). LCMS (APCI, *m/z*) 364, 366 (M + H^{+}). HPLC (method A): 97% (*t*R 9.5 min). Further elution afforded 2-(benzyl)-*N*-(2-chloropyrimidin-4-yl)-*N*,3-dimethyl-2*H*-indazol-6-amine (0.09 g, 18% yield) as the minor product as a clear gum. ^{1}H NMR (400 MHz): δ 7.95 (d, *J* = 6.1 Hz, 1 H), 7.83 (d, *J* = 8.8 Hz, 1 H), 7.56 (d, *J* = 1.0 Hz, 1 H), 7.27−7.39 (m, 3 H), 7.20−7.25 (m, 2 H), 6.91 (dd, *J* = 8.6, 1.8 Hz, 1 H), 6.29 (d, *J* = 6.1 Hz, 1 H), 5.65 (s, 2 H), 3.43 (s, 3 H), 2.63 (s, 3 H). LCMS (APCI, *m/z*) 364, 366 (M + H^{+}). HPLC (method A): 99% (*t*R 9.1 min).

Condensation of 2-(benzyl)-*N*-(2-chloropyrimidin-4-yl)-*N*,3-dimethyl-2*H*-indazol-6-amine and 3-aminobenzenesulfonamide following the procedure described in the preparation of **12b** afforded **12d** in 89% yield. ^{1}H NMR (400 Mz): δ 10.85 (br s, 1 H), 8.35 (br s, 1 H), 7.90 (d, *J* = 8.8 Hz, 2 H) 7.73 (br. d, *J* = 7.1 Hz, 1 H), 7.65 (s, 1 H), 7.56 (br s, 1 H), 7.43 (s, 2 H), 7.27−7.39 (m, 3 H), 7.24 (d, *J* = 6.8 Hz, 2 H), 6.97 (dd, *J* = 8.7, 1.6 Hz, 1 H), 6.00 (br s, 1 H), 5.67 (s, 2 H), 3.57 (s, 3 H), 2.66 (s, 3 H). LCMS (APCI, *m/z*) 498 (M − H^{+}). Anal. (C26H25N7O2S·HCl·H2O) C, H, N, Cl, S.

3-({4-[Methyl(2-methyl-2*H*-indazol-6-yl)amino]-2-pyrimidinyl}amino)benzenesulfonamide (12e) Hydrochloride. 2,4-Dichloropyrimidine (10 g, 67 mmol), 6-aminoindazole (8.9 g, 67 mol), and NaHCO3 (17.8 g, 211 mmol) were refluxed in 4:1 EtOH/THF (50 mL) under N2 for 16 h. The reaction was filtered while hot and the residue washed with hot EtOH (2 × 50 mL) and hot THF (25 mL). The filtrate was evaporated to yield a brown solid, which was triturated in EtOAc (50 mL) and filtered to give *N*-(2-chloro-4-pyrimidinyl)-

1*H*-indazol-6-amine (14.4 g, 87% yield) as a tan solid, which was used without further purification. ^1H NMR (400 MHz): δ 13.00 (br s, 1 H), 10.20 (s, 1 H), 8.19 (d, *J* = 5.8 Hz, 1 H), 8.11 (br s, 1 H), 8.00 (s, 1 H), 7.72 (d, *J* = 8.6 Hz, 1 H), 7.13 (dd, *J* = 8.6, 1.8 Hz, 1 H), 6.83 (d, *J* = 6.1 Hz, 1 H). LCMS (APCI, *m/z*) 246, 248 (M + H⁺). HPLC (method A): 89% (*t*_R 5.8 min).

To a stirred solution of *N*-(2-chloro-4-pyrimidinyl)-1*H*-indazol-6-amine (6.0 g, 24 mmol) in DMF (50 mL) was added Cs₂CO₃ (10.1 g, 31 mmol) and methyl iodide (3.0 mL, 48 mmol) at room temperature and the reaction stirred for 6 h. Additional Cs₂CO₃ (3.38 g, 10 mmol) and methyl iodide (0.46 mL, 7.4 mmol) were then added and the reaction stirred for an additional 16 h. The reaction mixture was poured into an ice−water bath (200 mL) and extracted with EtOAc (3 × 200 mL). Evaporation and silica gel column chromatography of the resulting crude product (hexanes/EtOAc) afforded *N*-(2-chloro-4-pyrimidinyl)-*N*,1-dimethyl-1*H*-indazol-6-amine (2.0 g, 30% yield) as a white solid following trituration with MeOH. ^1H NMR (300 MHz): δ 8.11 (d, *J* = 0.59 Hz, 1 H), 7.97 (d, *J* = 6.2 Hz, 1 H), 7.88 (d, *J* = 8.5 Hz, 1 H), 7.75 (s, 1 H), 7.08 (dd, *J* = 8.6, 1.7 Hz, 1 H), 6.30 (d, *J* = 6.0 Hz, 1 H), 4.03 (s, 3 H), 3.46 (s, 3 H). LCMS (ES, *m/z*) 274, 276 (M + H⁺). HPLC (method B): 94% (*t*_R 2.3 min). Further elution yielded as an oil which was taken up in Et₂O which on concentration yielded *N*-(2-chloro-4-pyrimidinyl)-*N*,2-dimethyl-2*H*-indazol-6-amine (1.6 g, 24% yield) an off-white solid. LCMS (ES, *m/z*) 274, 276 (M + H⁺). ^1H NMR (400 MHz): δ 8.42 (s, 1 H), 7.96 (d, *J* = 6.1 Hz, 1 H), 7.84 (d, *J* = 8.6 Hz, 1 H), 7.61 (s, 1 H), 6.96 (dd, *J* = 8.7, 1.6 Hz, 1 H), 6.27 (d, *J* = 5.8 Hz, 1 H), 4.19 (s, 3 H), 3.43 (s, 3 H). LCMS (APCI, *m/z*) 274, 276 (M + H⁺). HPLC (method A): 94% (*t*_R 7.0 min).

Condensation of *N*-(2-chloro-4-pyrimidinyl)-*N*,2-dimethyl-2*H*-indazol-6-amine with 3-benzenesulfonamide following the procedure described in the preparation of **12a** afforded **12e** in 90% yield as a white solid. ^1H NMR (300 MHz): δ 9.53 (s, 1 H), 8.56 (br s, 1 H), 8.40 (s, 1 H), 7.86 (d, *J* = 5.9 Hz, 1 H), 7.80 (d, *J* = 8.8 Hz, 2 H), 7.55 (s, 1 H), 7.34 (d, *J* = 2.5 Hz, 2 H), 7.25 (s, 2 H), 6.95 (dd, *J* = 8.72, 1.8 Hz, 1 H), 5.80 (d, *J* = 6.0 Hz, 1 H), 4.18 (s, 3 H), 3.50 (s, 3 H). LCMS (APCI, *m/z*) 408 (M − H⁺).

3-({4-[(1,2-Dimethyl-1*H*-benzimidazol-6-yl)(methyl)amino]-2-pyrimidinyl}amino)benzenesulfonamide (12f) and 3-({4-[(1,2-Di-methyl-1*H*-benzimidazol-5-yl)(methyl)amino]pyrimidin-2-yl}amino)benzenesulfonamide (12g). 2,4-Dichloropyrimidine and 2-methyl-1*H*-benzimidazol-5-amine were condensed to give (2-chloro-4-pyrimidinyl)-2-methyl-1*H*-benzimidazol-5-amine as a tan solid in 98% yield by the same procedure described in **12e**. ^1H NMR (400 MHz): δ 12.24 (br s, 1H), 10.03 (br s, 1H), 8.09 (d, *J* = 6.1 Hz, 1H), 7.81 (bs, 1H), 7.43 (d, *J* = 8.6 Hz, 1H), 7.17 (d, *J* = 7.6 Hz, 1H), 6.71 (d, *J* = 5.6 Hz, 1H), 2.47 (s, 3H). LCMS (APCI, *m/z*) (M + H⁺) 260, 262. HPLC (method A): 96% (*t*_R 4.0 min).

N-(2-Chloropyrimidin-4-yl)-1,2-dimethyl-1*H*-benzimidazol-5-amine was methylated by the same procedure described in **12b** to yield a 4:3 mixture of *N*-(2-chloro-4-pyrimidinyl)-*N*,1,2-trimethyl-1*H*-benzimidazol-6-amine and *N*-(2-chloropyrimidin-4-yl)-*N*,1,2-trimethyl-1*H*-benzimidazol-5-amine in 60% yield that was used as such in the subsequent reaction. LCMS (APCI, *m/z*) (M + H⁺) 288, 290. HPLC: 56% (*t*_R 4.3 min) and 42% (*t*_R 4.5 min).

The mixture of *N*-(2-chloro-4-pyrimidinyl)-*N*,1,2-trimethyl-1*H*-benzimidazol-6-amine and *N*-(2-chloropyrimidin-4-yl)-*N*,1,2-trimethyl-1*H*-benzimidazol-5-amine (0.20 g, 0.7 mmol) was combined with 3-aminobenenesulfonamide (0.10 g, 0.6 mmol) in *i*PrOH (5 mL) with 3 drops of aqueous HCl and stirred at 80 °C for 16 h. The reaction was quenched with solid NaHCO₃ while warm, then allowed to cool to room temperature and filtered. The filtrate was concentrated and the crude subjected to silica gel chromatography eluting with CH₂Cl₂ and MeOH to afford **12f** (0.050 g, 23% yield). ^1H NMR (400 MHz): δ 9.51 (s, 1H), 8.59 (s, 1H), 7.83 (d, *J* = 6.0 Hz, 1H), 7.77 (s, 1H), 7.60 (s, 1H), 7.52 (d, *J* = 1.9 Hz, 1H), 7.34 (m, 2H), 7.25 (s, 2H), 7.07 (dd, *J* = 8.4, 2.0 Hz, 1H), 5.69 (d, *J* = 6.2 Hz, 1H), 3.72 (s, 3H), 3.51 (s, 3H), 2.54 (s, 3H). LCMS (APCI, *m/z*) 424 (M + H), 446 (M + Na⁺). Further elution yielded **12g** (0.036 g, 16% yield). ^1H NMR (400 MHz): δ 9.50 (s, 1H), 8.59 (s, 1H), 7.80 (d, *J* = 6.1 Hz, 1H), 7.77 (s, 1H), 7.57 (d, *J* = 8.6 Hz, 1H), 7.46 (d, *J* = 1.8 Hz, 1H), 7.35

(m, 2H), 7.25 (s, 2H), 7.12 (dd, *J* = 8.4, 1.96 Hz, 1H), 5.62 (d, *J* = 5.7 Hz, 1H), 3.76 (s, 3H), 3.48 (s, 3H), 2.54 (s, 3H). LCMS (APCI, *m/z*) (M + H⁺) 424.

5-({4-[(2,3-Dimethyl-2*H*-indazol-6-yl)(methyl)amino]pyrimidin-2-yl}amino)-2-methylbenzenesulfonamide Hydrochloride (13). Condensation of 2*N*-(2-chloropyrimidin-4-yl)-*N*,2,3-trimethyl-2*H*-indazol-6-amine and 5-amino-2-methylbenzenesulfonamide following the procedure described in the preparation of **12b** afforded **13** in 81% yield. ^1H NMR (400 MHz, DMSO-*d*₆ + NaHCO₃): δ 9.50 (br s, 1H), 8.55 (br s, 1H), 7.81 (d, *J* = 6.2 Hz, 1H), 7.75 (d, *J* = 8.7 Hz, 1H), 7.69 (m, 1H), 7.43 (s, 1H), 7.23 (s, 2H), 7.15 (d, *J* = 8.4 Hz, 1H), 6.86 (m, 1H), 5.74 (d, *J* = 6.1 Hz, 1H), 4.04 (s, 3H), 3.48 (s, 3H), 2.61 (s, 3H), 2.48 (s, 3H). LCMS (APCI, *m/z*) 438 (M + H). Anal. (C₂₁H₂₃N₇O₂S·HCl) C, H, N, Cl, S.

Kinase Enzyme Assays. VEGFR enzyme assays for VEGGR1, VEGFR2, and VEGFR3 were run in homogeneous time-resolved fluorescence (HTRF) format in 384-well microtiter plates using a purified, baculovirus-expressed glutathione-*S*-transferase (GST) fusion protein encoding the catalytic c-terminus of human VEGFR receptor kinases 1, 2, or 3. Reactions were initiated by the addition of 10 μL of activated VEGFR2 kinase solution [final concentration, 1 nM enzyme in 0.1 M 4-(2-hydroxyethyl)-1-piperazineethane-sulfonic acid (HEPES), pH 7.5, containing 0.1 mg/mL bovine serum albumin (BSA), 300 μM dithiothreitol (DTT)] to 10 μL substrate solution [final concentration, 360 nM peptide, (biotin-aminohexyl-EEEEYFELVAKKKK-NH₂), 75 μM ATP, 10 μM MgCl₂], and 1 μL of titrated compound in DMSO. Plates were incubated at room temperature for 60 min, and then the reaction was quenched by the addition of 20 μL of 100 mM ethylene diamine tetraacetic acid (EDTA). After quenching, 20 μL HTRF reagents (final concentration, 15 nM Streptavidin-linked allophycocyanin (Perkin-Elmer), 1 nM Europium-labeled antiphosphotyrosine antibody (Perkin-Elmer) diluted in 0.1 mg/mL BSA, 0.1 M HEPES, pH 7.5) was added and the plates incubated for a minimum of 10 min. The fluorescence at 665 nM was measured with a Wallac Victor plate reader using a time delay of 50 μs.

Human Umbilical Vein Endothelial Cell (HUVEC) Proliferation Assay. The effect of kinase inhibitors on cell proliferation was measured using 5-bromo-2-deoxyuridine (BrdU) incorporation method using commercially available kits (Roche Diagnostics, Indianapolis, IN). HUVEC (Clonetics, Walkersville, MD) was seeded in medium containing 5% fetal bovine serum (FBS) in type 1 collagen coated 96-well plates and incubated overnight at 37 °C, 5% CO₂. The medium was aspirated from the cells, and various concentrations of the inhibitor in serum-free medium were added to each well. After 30 min, either VEGF (10 ng/mL) or bFGF (0.3 ng/mL) was added to the wells. Cells were incubated for an additional 72 h and BrdU (10 μM) was added during the last 18 to 24 h of incubation. At the end of incubation, BrdU incorporation in cells was measured by ELISA according to manufacturer's instructions. Data were fitted with a curve described by the equation, $y = V_{max}(1 - (x/(K + x)))$, where K is equal to the IC₅₀.

To assess tumor cell proliferation, cells were plated in culture medium containing 10% FBS and incubated overnight at 37 °C, 5% CO₂. Different concentrations of inhibitor in serum-free medium was added to each well to achieve a final concentration of 0.3% (v/v) DMSO and 5% FBS. Cells were incubated for 72 h at 37 °C, 10% CO₂. BrdU (10 μM final concentration) was added either 1.5 or 18 h prior to termination for tumor cells and HFF, respectively.

P450 Inhibition Assay. A range of concentrations of each compound dissolved in methanol in a 96-well plate were preincubated at 37 °C for 10 min in 50 mM potassium phosphate buffer (pH 7.4) containing 0.1 mg recombinant human CYP450 microsomal protein/mL (Cypex Ltd., UK) and the substrate. Following preincubation, 25 uL/mL of an nicotinamide adenine dinucleotide phosphate (NADPH) generating system (7.8 mg glucose-6-phosphate, 1.7 mg NADP, and 6U glucose 6-phosphate dehydrogenase/mL of 2% w/v NaHCO₃) was added to each well to start the reaction. Production of fluorescent metabolite was measured over 10 min time course using Cytofluor (Perkin-Elmer, US) plate reader. The rate of metabolite production (AFU/min) was deter-

mined for each concentration of compound and converted to a percentage of the mean control rates using Cytofluor software. The inhibitory potential (IC50) of each compound was determined from the slope of the plot using GraFit v5.08 (Erithacus software, UK). Miconazole was included as a positive control for each isozyme.

VEGFR2 Phosphorylation Assay. Phosphorylation of VEGFR2 was assessed in HUVEC stimulated with VEGF. HUVEC were plated in type-I collagen-coated 10 cm plates in Clonetics EGM-MV medium (Clonetics, Walkersville, MD) at $1.0-1.5 \times 10^6$ cells/plate. After 24 h, the confluent cells were serum starved overnight by replacing the growth medium with Clonetics EBM medium containing 0.1% BSA, 500 μg/mL hydrocortisone. Cells were treated with **13** at various concentrations for 1 h, followed by addition of 10 ng/mL VEGF or vehicle for 10 min. Cells were solubilized in lysis buffer. VEGFR2 was immunoprecipitated using antiflk-1 antibody and analyzed by sodium dodecyl sulfate polyacrylamide gel electrophoresis (SDS-PAGE) followed by Western blotting and detection with antiflk-1 or with antiphosphotyrosine (anti-P-tyr-biotin) antibody. The VEGFR2 phosphorylation level was quantified by densitometry and normalized to the total VEGFR2 level. For VEGFR2 phosphorylation in vivo, female Swiss nude mice were treated with a single oral dose of **13** prior to administration of VEGF$_{121}$ intravenously (15 μg/mouse). Five min after VEGF injection, mice were euthanized and their lungs were excised and snap frozen. Blood was collected for analysis of pazopanib levels in plasma. Frozen tissue was subsequently homogenized in lysis buffer and VEGFR2 phosphorylation was analyzed as described above.

Tumor Xenografts. Tumors were initiated by injection of tumor cell suspension in 8-12 week old nude mice. When tumors reached a volume of 100-200 mm^3, mice were randomized and divided into groups of eight. **13** was administered once or twice daily at 10, 30, or 100 mg/kg. Animals were euthanized by inhalation of CO$_2$ at the completion of the study. Tumor volume was measured twice weekly by calipers, using the equation: tumor volume (mm^3) = (length $\times$ width^2)/2. Results were routinely reported as % inhibition = 1 - (average growth of the drug treated population/ average growth of vehicle treated control population).

Matrigel Plug Assay. The bFGF/Matrigel angiogenesis assay was modified from the model described by Passaniti et al.[20] Female Swiss Nu/Nu mice were dosed once or twice orally on day 0 through day 4 with **13** (100, 30, or 10 mg/kg) or vehicle. On Day 0, a maximum of 1 h after compound administration, the anesthetized mice were injected subcutaneously at the ventral midline with 0.5 mL Matrigel (BD BioSciences) containing either 1 μg/mL bFGF or 0.05% BSA. On day 5, mice were euthanized and the Matrigel implants were excised and homogenized. Supernatant from homogenized samples were evaluated for angiogenic response by quantitative hemoglobin analysis using the Sigma 527-A Plasma hemoglobin assay. Hemoglobin values obtained via colorimetric assay were used to measure efficacy by defining percent inhibition as: 1 - ((Hb$_{Inhbitor-treated\ sample}$ - Hb$_{negative\ control}$)/(Hb$_{positive\ control}$Hb$_{negative\ control}$)) $\times$ 100. A two-tailed Student's t test as used to demonstrate statistical significance. Hemoglobin end points were used to determine percent of control for each sample.

Supporting Information Available: Assessment of purity for all target compounds by elemental analysis and/or HPLC, along with HPLC chromatogram tracings. This material is free of charge via the Internet at http://pubs.acs.org.

References

(1) Folkman, J. Angiogenesis: an organizing principle for drug discovery. *Nat. Rev. Drug Discovery.* **2007**, *6*, 273–286.

(2) Veikkola, T.; Karkkainen, M.; Claesson-Welsh, L.; Alitalo, K. Regulation of angiogenesis via vascular endothelial growth factor receptors. *Cancer Res.* **2000**, *60*, 203–212.

(3) Baka, S.; Clamp, A. R.; Jayson, G. C. A review of the latest clinical compounds to inhibit VEGF in pathological angiogenesis. *Expert Opin. Ther. Targets* **2006**, *10*, 867–876.

(4) (a) Caprioni, F.; Fornarini, G. Bevacizumab in the treatment of metastatic colorectal cancer. *Future Oncol.* **2007**, *3*, 141–148. (b) Ramalingam, S.; Belani, C. P. Role of bevacizumab for the treatment of non-small-cell lung cancer. *Future Oncol.* **2007**, *3*, 131–139.

(5) Kane, R. C.; Farrell, A. T.; Saber, H.; Tang, S.; Williams, G.; Jee, J. M.; Liang, C.; Booth, B.; Chidambaram, N.; Morse, D.; Sridhara, R.; Garvey, P.; Justice, R.; Pazdur, R. Sorafenib for the treatment of advanced renal cell carcinoma. *Clin. Cancer Res.* **2006**, *12*, 7271–7278.

(6) Chow, L. Q. M.; Eckhardt, S. G. Sunitinib: from rational design to clinical efficacy. *J. Clin. Oncol.* **2007**, *25*, 884–896.

(7) Sorbera, L. A.; Bolos, J.; Serradell, N. Pazopanib hydrochloride. Oncolytic, angiogenesis inhibitor, VEGFR-2 tyrosine kinase inhibitor. *Drug Future* **2006**, *31*, 585–589.

(8) Brignola, P. S.; Lackey, K.; Kadwell, S. H.; Hoffman, C.; Horne, E.; Carter, H. L.; Stuart, J. D.; Blackburn, K.; Moyer, M. B.; Alligood, K. J.; Knight, W. B.; Wood, E. R. Comparison of the biochemical and kinetic properties of the type 1 receptor tyrosine kinase intracellular domains: demonstration of differential sensitivity to kinase inhibitors. *J. Biol. Chem.* **2002**, *277*, 1576–1585.

(9) A homology model of VEGFR2 was created by using atomic coordinates, either publicly available from the RCSB or from in-house structures, for tyrosine kinases including c-FMS, Tie2, FGFR2, and insulin receptor. An in-house c-FMS structure was ultimately used as the primary model and for backbone regions of lower homology (e.g. inserts and deletions) or side chains of nonhomologous residues, appropriate RMS fitted coordinates from other X-rays were used where reasonable, followed by minimization.

(10) Shewchuk, L.; Hassell, A.; Wisely, B.; Rocque, W.; Holmes, W.; Veal, J.; Kuyper, L. F. Binding mode of the 4-anilinoquinazoline class of protein kinase inhibitor: X-ray crystallographic studies of 4-anilinoquinazolines bound to cyclin-dependent kinase 2 and p38 kinase. *J. Med. Chem.* **2000**, *43*, 133–138.

(11) Harris, P. A.; Cheung, M.; Hunter, R. N., III; Brown, M. L.; Veal, J. M.; Nolte, R. T.; Wang, L.; Liu, W.; Crosby, R. M.; Johnson, J. H.; Epperly, A. H.; Kumar, R.; Luttrell, D. K.; Stafford, J. A. Discovery and evaluation of 2-anilino-5-aryloxazoles as a novel class of VEGFR-2 kinase inhibitors. *J. Med. Chem.* **2005**, *48*, 1610–1619.

(12) Oprea, T. I. Property distribution of drug-related chemical databases. *J. Comput. Aid. Mol. Des.* **2000**, *14*, 251–264.

(13) Murray, M.; Wilkinson, C. F. Interactions of nitrogen heterocycles with cytochrome P-450 and monooxygenase activity. *Chem. Biol. Interact.* **1984**, *50*, 267–275.

(14) Kumar, R.; Knick, V. B.; Rudolph, S. K.; Johnson, J. H.; Crosby, R. M.; Crouthamel, M.-C.; Hopper, T. M.; Miller, C. G.; Harrington, L. E.; Onori, J. A.; Mullin, R. J.; Gilmer, T. M.; Truesdale, A. T.; Epperly, A. H.; Boloor, A.; Stafford, J. A.; Luttrell, D. K.; Cheung, M. Pharmacokinetic–pharmacodynamic correlation from mouse to human with pazopanib, a multi-kinase angiogenesis inhibitor with potent antitumor and antiangiogenic activity. *Mol. Cancer Ther.* **2007**, *6*, 2012–2021.

(15) Dev, I. K.; Dornsife, R. E.; Hopper, T. M.; Onori, J. A.; Miller, C. G.; Harrington, L. E.; Dold, K. M.; Mullin, R. J.; Johnson, J. H.; Crosby, R. M.; Truesdale, A. T.; Epperly, A. H.; Hinkle, K. W.; Cheung, M.; Stafford, J. A.; Luttrell, D. K.; Kumar, R. Antitumour efficacy of VEGFR-2 tyrosine kinase inhibitor correlates with expression of VEGF and its receptor VEGFR-2 in tumour models. *Br. J. Cancer* **2004**, *91*, 1391–1398.

(16) Sonpavde, G.; Hutson, T. E. Pazopanib: a novel multitargeted tyrosine kinase inhibitor. *Curr. Oncol. Rep.* **2007**, *9*, 115–119.

(17) Singh, R.; Argade, A.; Payan, D. G.; Molineaux, S.; Holland, S. J.; Clough, J.; Keim, H.; Bhamidipati, S.; Sylvain, C.; Li, W.; Rossi, A. B. Preparation of 2,4-pyrimidinediamines as IgE and/or IgG receptor modulators for treatment of allergic diseases, inflammatory conditions, and tissue destruction PCT Int. Appl. WO2003063794, 505, 2003.

(18) Thomas. A. P.; Hennequin, L. F. A.; Johnstone, C. Preparation of 4-anilinoquinazolines for use in the treatment of disease states associated with antiangiogenesis and/or increased vascular permeability PCT Int. Appl. WO9732856A1, 431997.

(19) Bergman, J.; Sand, P. Synthesis of indoles via ring closure of 2-alkylnitroaniline derivatives. *Tetrahedron* **1990**, *46*, 6085–6112.

(20) Passaniti, A.; Taylor, R. M.; Pili, R.; Guo, Y.; Long, P. V.; Haney, J. A.; Pauly, R. R.; Grant, D. S.; Martin, G. R. A simple, quantitative method for assessing angiogenesis and antiangiogenic agents using reconstituted basement membrane, heparin, and fibroblast growth factor. *Lab. Invest.* **1992**, *67*, 519–528.

(21) DeLano, W. L. *The PyMol Molecular Graphics System*; DeLano Scientific: San Carlos, CA, 2002; http://pymol.sourceforge.net/.